Published in final edited form as:

Proc Natl Acad Sci U S A. 2026 March 31; 123(13): e2602529123. doi:10.1073/pnas.2602529123.

Inorganic phosphate and the rapid mobilization of metabolic energy in neurons

Paul C. Rosen[1,2], **Shivang Sullere**[1,3], **Panhui Fu**[1], **Juan R. Martínez-François**[1], **Daniel J. Brooks**[1], **Erica Kim**[1], **Chenghua Gu**[1,3], **Gary Yellen**[1,*]

[1]Department of Neurobiology, Harvard Medical School, Boston, MA, USA 02115

[2]Department of Biology, Massachusetts Institute of Technology, Cambridge, MA, USA 02139

[3]Howard Hughes Medical Institute, Harvard Medical School, Boston, MA, USA 02115

Abstract

Neurons experience brief, intense periods of energy demand when they are excited, but how they rapidly coordinate energy expenditure with production is incompletely understood. Part of the difficulty has been measuring the levels of molecules involved in this metabolic response with spatiotemporal precision in single live cells. Here we engineered a quantitative fluorescent biosensor to monitor cytosolic inorganic phosphate (P_i), a fundamental component of energy metabolism that has a classically proposed but largely neglected role in activating glycolysis. Using two-photon fluorescence lifetime imaging, we observed millimolar increases in P_i within seconds of stimulating mouse neurons both *ex vivo* and *in vivo*. Drawing on results from metabolic modeling, biosensor imaging, and enzymology, we argue that P_i is a sensitive reporter of energy usage that potently links metabolic energy supply with demand in neurons. Quantitative live-cell imaging of P_i should be a valuable approach for studying bioenergetics more generally.

INTRODUCTION

Neuronal excitation is very energy-intensive, requiring adenosine triphosphate (ATP) to pump ions against their electrochemical gradients. To meet this demand, neurons rapidly mobilize metabolic energy, which comes from two major pathways.[1–5] The first is glycolysis, which rapidly breaks down glucose into pyruvate or lactate in the cytosol and produces two molecules of ATP. The second is oxidative phosphorylation, which oxidizes pyruvate (or other fuels) in mitochondria to generate a larger amount of ATP. In neurons, glycolysis temporarily outstrips oxidative phosphorylation in response to stimulation, providing fast and local energy resupply.[1,6–12]

What are the signals that link energy expenditure with the rapid activation of glycolysis in neurons? The textbook view of glycolysis regulation, derived almost entirely from *in vitro* experiments, is that metabolites associated with energy sufficiency (such as ATP,

*Correspondence to: Dr. Gary Yellen, gary_yellen@hms.harvard.edu.

COMPETING INTERESTS

G.Y. and Caroline D. Rae were co-signers of a group Letter to the Editor in the Journal of Neurochemistry (https://doi.org/10.1111/jnc.70230).

citrate, and glucose-6-phosphate) inhibit glycolysis enzymes, while metabolites associated with energy use (such as products of ATP hydrolysis and fructose bisphosphates) activate them. In excitable cells including neurons, most of this regulation is suspected to occur at the phosphofructokinase (PFK) step, which phosphorylates fructose-6-phosphate (F6P) to fructose-1,6-bisphosphate. The PFK reaction is a committed step of glycolysis, and PFK can sense many small-molecule signals associated with energy state.[1,13–15]

However, how this regulatory model pertains to glycolysis activation in living cells is unclear. One limitation is that the concentrations and dynamics of the candidate small-molecule regulators of glycolysis are poorly understood in neurons. For these putative effectors to actually regulate glycolysis, their concentrations should (1) resemble those required to have effects on glycolysis enzymes in vitro and (2) change with neuronal stimulation.[14] We previously showed that cytosolic citrate meets these criteria,[16] but making spatiotemporally precise metabolite measurements in complex physiological contexts is generally an unsolved problem. Ultimately, many such measurements will be required to assemble a fuller view of how neuronal glycolysis is activated during stimulation.

We focus in this paper on inorganic phosphate (P_i), a fundamental byproduct of ATP hydrolysis that is well poised to help coordinate the metabolic response to neuronal stimulation. Although P_i is now often neglected in regulatory schemes for eukaryotic glycolysis,[13] many decades ago P_i was shown to activate yeast, liver, and muscle PFKs *in vitro*. It is very likely that P_i also activates PFK from mammalian brain too, but this effect is incompletely understood.[14,17–22]

Evaluating the extent to which P_i regulates neuronal glycolysis requires knowing the concentration of P_i in the cytosol of neurons over the course of stimulation. Making this measurement has not been possible with existing techniques. Historically, magnetic resonance (MR) spectroscopy was used to measure changes in P_i *in vivo*, but this approach lacks cellular resolution and is difficult to quantify absolutely.[23–25] Coupled enzymatic assays and mass spectrometry have also been used to measure P_i, but these assays in general also lack cellular resolution and are destructive. Having a genetically encoded fluorescent biosensor for P_i could resolve these issues, as such a sensor could be targeted to specific subcellular spaces including the cytosol and monitored in single live cells over time.[26] Ideally, such a sensor would have only a single fluorescent protein and a pH-resistant, fluorescence-lifetime readout, permitting robust quantitation in complex contexts.[27,28] Only a dual-color P_i biosensor with small fluorescence changes currently exists, precluding quantitative imaging of neuronal P_i.[29,30]

Here, we engineered a quantitative single-color fluorescent biosensor for measuring P_i in the cytosol of single live cells and then used our measurements to argue that P_i helps to activate glycolysis during neuronal stimulation.

RESULTS

Inorganic phosphate is a sensitive indicator of energy utilization

Inorganic phosphate has a central role in neuronal energy metabolism: the ATPases that convert the energy of ATP hydrolysis into useful work yield both adenosine diphosphate (ADP) and P_i as products. P_i is the more durable product of ATPase action, because ADP is rapidly consumed by two other enzymes in cells (Fig. 1A). Creatine kinase (CK) rephosphorylates ADP to ATP by direct phosphate transfer from phosphocreatine (PCr). CK is highly expressed in all single neurons and neuron types in cortex and hippocampus, as well as in muscle cells.[31–33] This reaction mostly restores the ATP and ADP concentrations to their original values, but it does not reverse the P_i mobilization. Similarly, adenylate kinase (AK) takes two molecules of ADP and produces one of ATP and one of adenosine monophosphate (AMP). This temporarily restores the ATP concentration and the ATP/ADP ratio, but, because it involves direct phosphoryl transfer, it does not restore the mobilized P_i.[34,35]

Building on classic work by Connett[36], we formalized the effect of these enzyme systems with a simple equilibrium model to show the evolution of changes in their substrates with various degrees of energy depletion (spreadsheet in Supporting Information). The coupled AK/CK equilibrium illustrates the sensitivity of P_i as an indicator of energy consumption. As energy is consumed, PCr reserves are depleted first, and then ATP reserves are depleted afterwards (Fig. 1B), consistent with observations in the brain during hypoxia and in single stimulated muscle fibers.[37–41] Across both of these phases in our model, P_i changes linearly. During periods of acute energy use, changes in P_i are likely several-millimolar while those of other ATP hydrolysis products such as AMP are likely very low-micromolar (Fig. 1C). The model is certainly a simplification because it does not include the effects of other enzymes like AMP deaminase (which prevents accumulation of AMP, preserving the energy available from ATP hydrolysis; Fig. S1), or of possible ADP buffering by binding to cellular enzymes.[42] Nevertheless, it motivates measuring P_i as signal of energy usage in neurons.[36]

Pi-Tq, a quantitative lifetime-readout biosensor for inorganic phosphate

Despite the centrality of P_i in energy metabolism, measuring it in single living cells has been challenging. To address this issue, we engineered a quantitative biosensor for P_i with a fluorescence-lifetime readout. We began with a previously reported Förster resonance energy transfer biosensor for P_i, which had only a marginal change in fluorescence lifetime in response to P_i (Fig. S2A).[29] We converted this sensor into a single-color lifetime-readout sensor for P_i by inserting circularly permuted mTurquoise (a fluorescent protein commonly used in lifetime-readout biosensors) into a predicted P_i-sensitive loop region of a phosphate-binding protein (PiBP) scaffold (Fig. 2A).[16,43–45] We varied the position, lengths, and identities of the connections between the fluorescent protein and the PiBP to generate a P_i biosensor with fluorescence-lifetime contrast.

After several rounds of screening, we obtained a sensor with a ~0.5 ns increase in fluorescence lifetime in response to P_i, which we named Pi-Tq (Fig. 2B, S3). Pi-Tq was pH-resistant between pH 6.8 – 7.7 and bound to P_i with a $K_{apparent}$ of ~3 mM at room

temperature, making it well-suited for use in the cytosol (Fig. 2B).[46] The sensor was specific for P_i relative to the related polyatomic ions sulfate and nitrate as well as to pyrophosphate and PCr, which have terminal phosphate groups (Figs. 2C,D). The sensor is used most effectively with a fluorescence-lifetime readout, but it also has modest changes in fluorescence intensity, similar to other sensors built from cyan fluorescent proteins (Figs. S2C–E).

To enable sensor quantitation in physiological contexts, we performed a series of Pi-Tq calibrations using two-photon fluorescence lifetime imaging (2pFLIM) at elevated temperatures. Such calibrations are important because both binding affinity and fluorescence lifetime can be temperature-sensitive in lifetime-readout biosensors.[16] At 34°C, Pi-Tq bound to P_i with a $K_{apparent}$ of ~4 mM; the P_i-free and P_i-saturated Pi-Tq lifetimes measured for purified protein and for permeabilized HEK293T cells were very similar (Fig. 2E). Although the P_i-free and P_i-saturated lifetimes were temperature-sensitive (declining 0.02–0.03 ns/°C increase), the $K_{apparent}$ of the sensor was relatively temperature-insensitive within the tested temperature range (Fig. S4). These results set the stage for quantitative imaging of P_i.

Activity-dependent inorganic phosphate dynamics in neurons

We deployed Pi-Tq to measure P_i in the cytosol of neurons. We focused almost entirely on dentate granule cells (DGCs), which have been a model system for understanding the relationship between neuronal activity and metabolism.[6,7,11,16] We prepared acute hippocampal brain slices from juvenile mice previously injected with an adeno-associated virus (AAV) expressing Pi-Tq and imaged them with 2pFLIM, allowing quantitative single-color imaging. The baseline Pi-Tq lifetime in DGCs was 1.71 ± 0.02 ns (Fig. S5A). This lifetime corresponds to a baseline P_i concentration of ~4 mM, consistent with prior estimates of brain P_i (Fig. 2E).[35,46–48] The baseline fluorescence lifetimes did not vary systematically with the starting fluorescence intensity of Pi-Tq, suggesting that sensor expression is not limiting for accurate lifetime estimation in this preparation (Fig. S5B). Decreasing or increasing extracellular P_i led to small, slow decreases and increases in sensor lifetime, respectively, likely reflecting P_i transport (Figs. S5C,D).[46] These experiments demonstrate the suitability of Pi-Tq for studying neuronal P_i metabolism.

Inorganic phosphate dynamics in mouse neurons *ex vivo*: We asked how neuronal activity affects P_i levels in the neuronal cytosol. We suspected that stimulation would increase P_i levels as energy is consumed (Fig. 1B), but the magnitude and dynamics of this increase were not known. Neuronal activity in physiological conditions often evokes little-to-no changes in fluorescent biosensors for cytosolic ATP or the ATP:ADP ratio, perhaps because these parameters actually change little or because the sensors for them are suboptimally tuned for use in physiology (Fig. 1B).[49–57]

To determine how neuronal activity changes cytosolic P_i, we imaged Pi-Tq-expressing DGCs over the course of two different types of stimulation, co-monitoring the red Ca^{2+} sensor RCaMP1h as a control (stimulation elevates cytosolic Ca^{2+}).[58] We first strongly depolarized neurons with a 1 min pulse of artificial cerebrospinal fluid (aCSF) containing 50 mM KCl, leading within seconds to an increase in Pi-Tq lifetime from 1.72 ± 0.04 to

1.77 ± 0.04 ns (Figs. 3A,B). Applying our purified protein calibration, we estimate that this increase corresponds to a change in cytosolic P_i from ~4 mM to ~8 mM (Fig. 2E). The size of the KCl-evoked change in Pi-Tq lifetime was not related to the starting Pi-Tq lifetime (Fig. S5E). Curiously, we almost always observed that after rising sharply in response to stimulation and then decaying, the Pi-Tq lifetime undershoots its initial baseline before normalizing over a few minutes (Fig. 3A). We also stimulated neurons electrically, providing a brief and mild depolarization relative to KCl. Electrical stimulation elicited slightly a smaller transient than did KCl, with the Pi-Tq lifetime promptly rising from 1.72 ± 0.02 to 1.75 ± 0.01 ns (Figs. 3C,D), which corresponds with a change in P_i from ~4 mM to ~6 mM.

Inorganic phosphate dynamics in mouse neurons *in vivo*: We obtained similar results when we imaged Pi-Tq *in vivo* using 2pFLIM. We expressed Pi-Tq in adult mice implanted with a cranial window, and then imaged barrel cortex in awake head-fixed mice. Similar to DGCs in brain slices, the baseline lifetime of Pi-Tq lifetime expressed in cortical neurons *in vivo* was ~1.7 ns (Fig. 4A), indicating that the sensor could detect both increases and decreases in P_i.

We used an optogenetic approach to test how neuronal activity changes P_i levels *in vivo*. We co-expressed Pi-Tq along with the opsin ChrimsonR, which depolarizes neurons in response to red light illumination.[59] Brief (30s) optogenetic stimulation promptly led to a millimolar-level increase in P_i, as the Pi-Tq lifetime increased by 0.08 ± 0.02 ns (Figs. 4B,C). Similar to our observations in KCl-stimulated DGCs, the initial rise in Pi-Tq lifetime was quickly followed by a pronounced undershoot before the lifetime returned to baseline over a few minutes. Red light did not evoke a change in Pi-Tq lifetime in the absence of opsin expression, indicating that the lifetime changes are due to optogenetic stimulation of neuronal activity and not to off-target effects of illumination (Fig. S6). Taken together, these experiments demonstrate that neuronal activation rapidly leads to several-millimolar increases in cytosolic P_i.

Inorganic phosphate and the regulation of neuronal glycolysis

To what extent, if any, might the stimulation-induced changes in P_i contribute to the activation of glycolysis in neurons? We addressed this question in two ways. First, neuronal activity leads to a dip in the cytosolic concentration of the glycolysis inhibitor citrate, which could in theory be the major regulatory signal for glycolysis in neurons.[16] We asked whether it is necessary to invoke the actions of effectors beyond citrate to explain the activation of neuronal glycolysis. Second, we compared the P_i concentration changes that we measured to the biochemical properties of P_i-sensitive glycolytic enzymes.

Multiple controls of glycolysis in neurons: To test whether the stimulation-dependent dip in citrate is necessary for glycolysis activation in neurons, we needed an experimental system where we could selectively remove the citrate change in response to stimulation. We built on our prior work where we showed that depleting the mitochondrial calcium uniporter (MCU) diminished the stimulation-induced change in citrate.[16] However, the citrate transient was not completely eliminated in these experiments, probably because there was some remaining MCU activity.

We reasoned that depolarization in the absence of extracellular Ca^{2+} might completely abolish the citrate transient, which would permit a clearer test of the necessity of citrate changes in neuronal glycolysis activation. We therefore performed a series of stimulation experiments in the presence or absence of Ca^{2+}. As readouts, we monitored in parallel experiments four different quantitative fluorescent biosensors: for citrate, P_i, and two components of glycolysis.

We began by testing whether we could eliminate the decrease in citrate caused by neuronal activity. Consistent with our prior work, stimulating neurons in the presence of external Ca^{2+} led to a strong dip in citrate, but without external Ca^{2+} there was remarkably no detectable stimulation-dependent change in citrate (Figs. 5A, S7A).[16] Under the same conditions, we found that the P_i change was largely intact (Fig. 5B, S7B), consistent with previous observations that changes in calcium are less important than Na^+/K^+-ATPase activity for activating glycolysis in DGCs.[7,35] Therefore, while the stimulation-induced change in citrate depends on Ca^{2+}, the P_i change does not.

Was glycolysis still activated even in the absence of a dip in cytosolic citrate levels? We imaged two lifetime-readout biosensors probing different aspects of glycolysis to address this question. We first imaged the cytosolic NADH/NAD^+ ratio (which increases when glycolysis is activated) using the lifetime-readout biosensor Peredox.[6] Similar to previous results, there was a clear NADH/NAD^+ transient in response to stimulation both in the presence and absence of extracellular Ca^{2+}, although the transient was ~50% smaller without external Ca^{2+} (Fig. 5C, S7C).[7] As an orthogonal measure of glycolysis activation, we also imaged a lifetime-readout glucose biosensor in our stimulation paradigm (Fig. S8). Previously, we observed small dips in glucose when neurons are activated, reflecting increased glucose consumption as a result of increased glycolysis.[6] Glucose levels dipped in response to stimulation, both in the presence and absence of extracellular Ca^{2+} (Figs. 5D, S7D). Taken together, these results are consistent with the interpretation that factors in addition to citrate regulate glycolysis in neurons.

Beyond P_i (which changes largely Ca^{2+}-independently), there are not many plausible options for what such effectors might be. Clearly the change in citrate is not required for the rapid activation of glycolysis in neurons (Fig. 5), and we previously ruled out a requirement for changes in cytosolic Ca^{2+} and AMPK signaling in this process, as well.[7] In many neuronal preparations, baseline ATP levels are 3 – 4 mM, which will inhibit PFK; stimulation elicits only small dips in [ATP].[51,52,56,60,61] Others have argued that because neurons have very low levels of PFKFB3, they may lack appreciable fructose-2,6-bisphosphate (F2,6bP), a potent activator of PFK.[13,14,62] Finally, AMP levels are likely too low to meaningfully regulate glycolysis enzymes in acute settings (Figs. 1C, S1C).[17,22,63] P_i is therefore a strong candidate for regulating neuronal glycolysis.

Activation of brain PFK by inorganic phosphate: If P_i indeed stimulates neuronal glycolysis, where in glycolysis might it act? According to the literature, P_i can stimulate at least four distinct steps in glycolysis (Fig. 6A). We focused on one of these steps: the activation of PFK by P_i. Although P_i *can* activate PFK in vitro, whether P_i *does* activate PFK in neuron-like conditions is not clear.[17–22]

We asked how P_i activates brain PFK under near-physiological conditions. We used a coupled enzyme assay to test how P_i activates recombinant platelet PFK isoform (PFKP), which is likely the dominant isoform in mouse brain.[31,64] We performed our assays with high ATP (3.5 mM), low F6P (0.1 mM), and 0.1 mM free citrate to mimic the baseline state of the neuronal cytosol to the best of our knowledge.[16,35,51,52,60,65,66]

Remarkably, P_i alone was sufficient to activate PFKP more than sixty-fold (Fig. 6B), even in the complete absence of other activators such as F2,6bP and AMP. The $K_{apparent}$ for P_i was ~4 mM, which overlaps well with the levels that we measured in neurons. Going from a ~4 mM P_i baseline to a 6–8 mM peak level would strongly activate PFK. The P_i-dependent activation of PFKP was highly cooperative (Hill coefficient of ~7.5), which is consistent with previous observations and reflects the strongly inhibited state of the enzyme in the absence of P_i in our experimental conditions. Although a physiological decrease in citrate strongly activated PFK at low P_i, it did not activate much at higher P_i, possibly because one of the PFK P_i-binding sites overlaps with the citrate-binding site (Fig. 6C).[67–70] The enzymology supports an important role for P_i in the activation of neuronal glycolysis.

DISCUSSION

By engineering Pi-Tq, a biosensor for P_i with a quantitative fluorescence-lifetime readout (Fig. 2), we were able to measure cytosolic P_i levels in neurons over the course of stimulation (Figs. 3,4). The P_i changes that we measured are consistent with the proposal that P_i, an obligate and sensitive signal of energy demand, functions as a feed-forward signal to activate neuronal glycolysis (Figs. 1, 3–6). Despite having been studied for many years, there are still many rich outstanding questions about P_i.[71–79]

Features of the P_i transients seen with neuronal stimulation

The initial ATP consumption in an excitable cell containing the PCr/CK system is offset by rephosphorylation of ADP at the expense of PCr, such that [PCr] declines in advance of [ATP], as seen in MR spectroscopy experiments both in muscle and brain.[38–41] This behavior makes ATP a late reporter of energy stress – but, as shown in Figs. 1, 3, and 4, P_i changes very promptly and by millimolar increments. This makes P_i an excellent indicator (both to scientists and to the cell) of fast energy mobilization in neurons, particularly at early stages.

A curious feature of P_i behavior, following its increase with strong stimulation, is an undershoot below the original level. We doubt that this undershoot is an artifact since we observed it both in DGCs stimulated with KCl in acute brain slices and in cortical neurons stimulated optogenetically *in vivo* (Figs. 4A,5C). It is not surprising that previous methods to detect P_i, which basically cannot resolve levels in single cells over time, would have missed such a phenomenon. Assuming that it is real, the origins of the undershoot are not trivial to explain. One possibility is that mitochondrial Ca^{2+} influx leads to the formation of insoluble Ca-phosphate complexes, which sequester P_i in the matrix and then are slow to re-dissolve.[80,81] Testing this idea is challenging, given the absence of methods to dynamically quantify Ca-phosphates in cells. A second, not-mutually-exclusive possibility is that after the initial transient, there is a brief “overcharging” of energy reserves

in the cytosol, post-stimulation, that leads to increased sequestration of P_i in ATP and PCr. Consistent with this idea, others have observed transient overshoots in phosphocreatine levels after stimulation using MR spectroscopy.[82] Future work will be required to develop orthogonal means to test the reality of the P_i undershoot and then to distinguish between these (and other) mechanistic possibilities.

P_i regulation of PFK

PFK is generally considered a key control point for glycolysis, and consistent with earlier reports, we see strong activation of PFK by P_i.[17–22] With physiological concentrations of ATP, citrate, and F6P, P_i changes within the physiological range activate PFKP steeply. This high cooperativity (Hill coefficient ~7.5, Fig. 6B) is remarkable but not completely surprising, as P_i binds to two sites on each monomer of PFKP and the protein is tetrameric.[68,69] Others have seen strong cooperativity of PFK with respect to its substrate F6P.[17,18,20,22,62] Because the effect of PFK activators is typically to oppose the effect of PFK inhibitors, the presence of ATP and citrate is critical to observe the P_i cooperativity; in fact, one of the P_i-binding sites is almost certainly overlapping with the citrate inhibitory site.[68] Learning the molecular details of how P_i can activate PFK is an important future goal.

The details of the P_i dependence of PFK are exquisitely sensitive to the concentrations of activators, inhibitors, and substrate. One can imagine that slower forms of regulation, both of baseline P_i and of other ligand concentrations (such as F2,6bP), may tune the position of this P_i-dependence curve to match the basal metabolic needs and to poise the transient response to be a steep function of energy usage as reported by P_i accumulation. At a physiological level, it will be of interest to understand how cells execute this calibration (both acutely by small molecules and more slowly by signaling), and whether different types of cells have different P_i-response setpoints. Addressing this question will almost certainly require measurements of additional PFK effectors, to more tightly constrain the conditions for in vitro assays. Whether there is a finer level of PFK regulation within particular regions of the cytosol (as has been proposed) also remains to be determined.[83,84]

Inorganic phosphate as a distributed regulator of the fast response to energy demand

PFK is not always the key regulatory and control step in glycolysis. As metabolic control analysis and many experiments demonstrate, control and regulation of glycolysis can occur at multiple steps in the pathway.[85] The exact steps with strong metabolic control are controversial, partly because which steps exert flux control depends critically on the detailed physiological state of the cell (e.g. the concentrations of all the metabolic intermediates and regulators). For instance, phosphoglycerate kinase (PGK) can be a control point in neurons incubated in very low glucose levels, and GAPDH has been reported to be a control point in cancer cells.[86,87]

Because P_i can influence many of these steps (Fig. 6A), it may act a robust distributed regulator of glycolysis.

- We have shown here that P_i can directly act on PFKP (and probably on heteromers of different PFK isoforms, as well). The low reported PFKFB3 activity will actually tend to give PFK *more* control of flux, by throttling its

activity to a lower baseline level. Citrate also acts on this step, as can F2,6bP and AMP, if they were to get high enough.[14,16,61]

- The PGK step shown to exert flux control with low [glucose] is not a direct target of P_i, but P_i can increase PGK flux by shifting the preceding GAPDH equilibrium (even if that step is so rapid as to not itself have any flux control). P_i is a substrate of GAPDH and pushes the equilibrium toward the product 1,3-bisphosphoglycerate, which is a substrate for PGK. Several other factors, including the NADH/NAD^+ ratio and the ATP/ADP ratio, could also influence flux control at the PGK step.[48,86,88]
- Glycogenolysis in neurons is not widely appreciated, but it clearly plays a vital role in neuronal energy management.[89–91] Glycogen phosphorylase uses P_i directly as a substrate and it is sensitive to P_i in the millimolar range.[92] This step is also influenced by AMP and by calcium-calmodulin effects both on phosphorylase and on the regulatory phosphorylase kinase.[93,94]
- Product inhibition of hexokinase by glucose-6-phosphate can possibly be strong enough to give HK a measure of flux control, and the degree of product inhibition is reported to be regulated by P_i (though this may not occur much in the physiological range).[95–97]

P_i can influence all of these steps, while other effectors affect only one or two steps at most. If chronic influences augment AMP or F2,6bP, then their targets would have less influence on flux, shifting acute flux regulation to the other steps that are (still) P_i dependent.

We focused on a role for P_i in stimulating glycolysis as part of the mechanism linking energy expenditure with energy production, but P_i is well known to stimulate mitochondrial metabolism as well. Although the mechanistic details of this stimulation are not completely understood, P_i likely directly stimulates the electron transport chain and glutaminase within mitochondria.[98,99] Disentangling these additional effects will require measuring P_i within the mitochondrial matrix. Even though we were able to use Pi-Tq effectively in the cytosol of stimulated neurons, it would benefit from additional engineering to enlarge its change in fluorescence lifetime and signal-to-noise ratio to help address this and other questions.

Future needs for a thorough understanding of the rapid mobilization of metabolic energy in neurons

While P_i is the best available monitor for fast energy utilization, studies of brain metabolism would benefit from additional biosensor tools. PCr levels are an excellent measure of immediate energy reserve and its depletion. While MR spectroscopy can reveal these levels in brain at a coarse spatial scale, and mass spectrometry imaging can see them at near-cellular resolution, there are no tools for measuring PCr dynamically at a cellular or subcellular level.[100,101] A fluorescent biosensor to measure PCr concentration would report on energy reserve, and a sensor to measure the ratio of PCr/Cr, roughly in the range of 4 to 0.2, might report energy status more reliably than the corresponding high ATP/ADP ratios likely to prevail in the cytosol (the CK equilibrium keeps the ATP/ADP ratio ~100x higher than the PCr/Cr ratio).[34–36] Existing ATP/ADP ratio sensors are saturated at such

high levels.[49] A sensor for free ADP in the low micromolar range might also be revealing for local energy usage.[42] Making sensors to measure these and other molecules relevant for bioenergetics is required for a thorough and panoramic view of both neuronal energy budgets and energy dynamics in physiological settings.[102]

There is also a need for studies of the allosteric behavior of glycolytic enzymes under near-physiological conditions. Elegant enzymological studies of glycolytic enzymes over many decades have focused (appropriately) on discovering the full range of regulation and the mechanisms of interaction between allosteric effects. This has led, for instance, to the use of non-physiological concentrations of regulatory ligands (e.g. 0.1–0.3 mM ATP, to avoid too much inhibition, and >0.25 mM F6P, to observe effects of other ligands on V_{max}).[17–22,63,66] But looking forward, more focus is needed on studies that use ligand concentrations within the physiologic range, so far as we can determine them. Much as Connett (in 1988!) advocated for increased study of P_i as a regulator of PFK, we hope that such future studies can facilitate better understanding of the physiological behavior of many glycolytic enzymes.[36]

METHODS

Modeling:

The equilibrium model largely reproduced previous work by Connett, who considered the coupled equilibrium between creatine kinase (CK) and adenylate kinase (AK) with adjustments for H^+, Mg^{2+}, and K^+. We corrected an inversion error in one equation of ref. 36. The model parameters and calculations are in an Excel file (Software S1).

Kinetic modeling was performed using COPASI[103], with initial concentrations and equilibrium constants matching the Connett model. We incorporated AMP deaminase in our model and had ATP hydrolysis begin at t=0 while not allowing ATP re-synthesis (so that ATP could be consumed). We assumed that all enzymes are sub-saturation and that CK and AK are fast compared with ATP hydrolysis. The parameters for the kinetic model are given in the form of a COPASI file and an equivalent SBML file in the Supporting Information (Software S2).

Molecular biology:

Chemicals were obtained from Sigma-Aldrich, unless otherwise noted. Oligonucleotides were obtained from Integrated DNA Technologies or Azenta Life Sciences. Plasmids were verified by whole-plasmid sequencing. pRsetB-TEV-PiTq (#248768), pAAV-CAG-PiTq (#248769), pAAV-CAG-SweetieTS2 (#252286), and pAAV-hSyn-PiTq (#248770) are available from Addgene.

Sensor development:

We engineered a lifetime-readout phosphate sensor by fusing a PiBP from *Synechococcus* with mTurquoise. We used the 1.6 m variant as starting scaffold for sensor construction, given its predicted suitability for sensing physiological concentrations of cytosolic phosphate. We used AlphaFold3 (https://alphafoldserver.com/welcome) to predict the PiBP

structure (iPTM = 0.81).[104] We targeted a loop region at the back of the putative phosphate-binding pocket for coupling to the fluorescent protein. We varied the lengths and identities of the engineered amino acid connections between the PiBP and the fluorescent protein, preparing variable linker libraries by Gibson Assembly and expressed them in 96-well plate format in *Escherichia coli* BL21(DE3), as described. For screening, we used a 96-well crude purification method that we have previously described in detail.[16] Fluorescence lifetimes were measured in the absence and then in the presence of P_i. Variants exhibiting lifetime changes were Sanger sequenced, guiding the design of the next round of linker variants to screen.

Initially, we circularly permuted the PiBP and inserted it into split mTurquoise. After several rounds of screening, we obtained a prototype sensor that exhibited changes in fluorescence lifetime in response to P_i, but only over many minutes. We then inverted the topology of the sensor, inserting circularly permuted mTurquoise into the PiBP instead. Re-optimizing the linkers connecting mTurquoise with PiBP in this configuration eventually led to a variant with a ~0.5 ns change in fluorescence lifetime in response to P_i, which we named Pi-Tq. The sequence of the sensor is given in Fig. S3.

Protein purification:

Sensor protein was expressed recombinantly in *E. coli* BL21(DE3), largely as we have described before.[16] We expressed both a standard 6xHis-tagged version and a version where the N-terminal affinity tag could be cleaved off by tobacco etch virus (TEV) protease; the tagged and tag-free versions had identical binding properties to each other. Sensor-expressing bacteria were grown in 100 mL of either Luria Broth or Terrific Broth with shaking at 200 rpm at 37°C overnight. Protein production was induced with 0.5 mM isopropyl β-D-1-thiogalactopyranoside at room temperature with shaking at 200 rpm for an additional 24 h. After induction, bacteria were harvested by centrifugation at 4,000 × g for 15 min.

An important modification to our prior procedure is that all proteins were purified in Pi-free buffers. We re-suspended bacterial pellets in 10 mL of lysis buffer [50 mM HEPES (pH 8.0), 300 mM NaCl, 10 mM imidazole], supplemented with 1 tab cOmplete mini EDTA-free protease inhibitor cocktail per 10 mL lysis buffer and ~0.1 mg/mL lysozyme. After brief sonication on ice, we added 1 μL Pierce Universal Nuclease to the lysate, which was then incubated on ice for ~15 min.

The lysate was centrifuged for 10 min at 21,000 × g, and the supernatant was applied to Ni^{2+}-nitrilotriacetic acid resin by gravity flow (Qiagen). Bound protein was washed with 10 mL of lysis buffer, followed by 10 mL of lysis buffer with 30 mM imidazole. Pi-Tq was eluted with 5 mL of lysis buffer supplemented with 500 mM imidazole, concentrated using 30 kDa-cutoff spin concentrators (Amicon), and then exchanged into assay buffer [25 mM MOPS (pH 7.4), 50 mM KCl, 50 mM NaCl, 0.5 mM $MgCl_2$, 2.5% glycerol, 0.5 mM dithiothreitol]. A typical yield was 5–10 mg of sensor per 100 mL of expression culture.

For tag-cleaved preps, we exchanged purified, TEV-cleavable protein into a TEV cleavage buffer [50 mM Tris-HCl (pH 7.5), 0.5 mM EDTA, 1 mM DTT]. Cleavage was performed

overnight at room temperature with 50 units of TEV protease (New England Biolabs). Tag-cleaved Pi-Tq was purified by reverse Ni^{2+}-affinity chromatography and then concentrated and buffer-exchanged. All assays were performed with freshly purified protein.

One-photon excitation fluorescence lifetime assays:

Binding assays were performed in black 96-well plates with ~500 nM sensor protein resuspended in assay buffer with varying amounts of sodium phosphate. We used the assay buffer described above, supplemented with sodium phosphate and adjusted to the desired pH. As previously described, fluorescence lifetimes were measured using a PR1 plate reader connected to a FLS 980 Spectrometer and illuminated with a Fianium WhiteLase Micro pulsed supercontinuum laser filtered by an adjustable bandpass interference filter (excitation wavelength set to 435 ± 17 nm and the emission set to 505 ± 20 nm). Fluorescence lifetimes were determined using double-exponential fitting in MATLAB R2014b; we did not restrict the fits to the first 8 ns of arrived photons. Binding data were fit using a Hill equation (fixed Hill slope of 1) in GraphPad Prism 10.

Photophysical characterization:

Excitation (excitation from 350–480 nm, with emission fixed at 520 nm, 2 nm step size) and emission (excitation fixed at 400 nm, monitoring emission from 440–650 nm, 2 nm step size) spectra were collected using Biotek Synergy H1 plate reader. Fluorescence intensity phosphate titrations were also performed using a Biotek Synergy H1 plate reader, with excitation at 440 nm and emission at 500 nm. Extinction coefficients were determined using Beer's law ($A=\varepsilon cl$), using absorbance at 440 nm measured via a Nanodrop UV-Vis spectrophotometer and protein concentration as determined by using a bicinchoninic acid assay, so the reported extinction coefficient may be a slight underestimate. P_i-free and P_i-saturated (100 mM) quantum yields were determined using a Photon Technologies International fluorometer in relation to a calcium-saturated TqFLiTS reference (QY = 0.75).[44] We used Pi-Tq that had not been TEV-cleaved for photophysical assays.

Two-photon excitation calibration:

Calibrations of purified, tagless Pi-Tq were performed in sealed glass capillaries, loaded with 1–10 μM protein in assay buffer and with varying levels of P_i. The capillaries were heated to 32, 34, or 37°C. Three independent protein preparations were imaged using a customized two-photon excitation fluorescence lifetime microscope, which has previously been described in detail. Briefly, the objective lens was an Olympus 60X LUMPlanFL (NA 1.0), with digital zoom set to 1x. Fluorescence emission was split using a FF562-Di03 dichroic mirror, and then bandpass filtered for green (FF01–510/84) and red (FF01–641/75) channels. Excitation was at 820 nm. Fluorescence lifetimes were determined by double-exponential fitting in MATLAB R2014b as described previously, and the binding titration was fit with a Hill equation in GraphPad Prism 10.

We also performed a rough in-cell calibration of Pi-Tq at low and high P_i, adapting a previously used approach.[16,105] HEK293T cells were maintained at 37°C, 5% CO_2 in DMEM supplemented with 10% serum, 100 IU mL^{-1} penicillin, and 100 μg mL^{-1} streptomycin. The day before transfection, ~100,000 cells were plated on clean, protamine-

coated glass coverslips in a six-well plate. The next day, the cells were transfected with ~500ng/well of pAAV-CAG-PiTq using a 3:1 ratio of X-tremeGene9 and then imaged 2–5 days post-transfection. Cells were permeabilized at 34°C in an in-cell calibration buffer [140 mM K-Gluconate, 10 mM NaCl, 10 mM HEPES, 1 mM EGTA, 1.324 mM $MgCl_2$, 0.346 mM $CaCl_2$, pH 7.35] with 45 μM β-escin for ~10 min, until the cells had rounded completely. The permeabilized cells were then incubated at 34°C in in-cell calibration buffer containing either 0- or 100-mM sodium phosphate for ~15 additional minutes, until the fluorescence lifetime stabilized. The imaging set-up was the same as for the purified protein calibration, except that the excitation wavelength was 790 nm.

Acute brain slice imaging:

Female and male wild-type C57BL/6N mice between the ages of P14 and P28 were used. Animals were bred in-house in ventilated cages within a barrier facility, which maintained 12 hr light/dark cycle, regulated cage temperature (24°C) and humidity (53%) and provided *ad libitum* access to water and food (Picolab Rodent Diet 5053). All experiments followed approved IACUC protocols and the NIH Guide for the Care and Use of Laboratory Animals and Animal Welfare Act. All procedures were approved by the Harvard Medical Area Standing Committee on Animals.

Brain slice imaging was performed similarly to prior studies.[7,16] Adeno-associated viruses for pAAV-CAG-PiTq (AAV8 serotype, 3.1E13 GC/mL), pAAV-CAG-CitA-Tq-LR (AAV8 serotype, 4.8E13 GC/mL), pAAV-CAG-Peredox (AAV8 serotype, 1.4E13 GC/mL), pAAV-CAG-SweetieTS2 (AAV8 serotype, 1.1E13 GC/mL), and pAAV-hSyn-RCaMP1h (AAV9 serotype, 1.2E13 GC/ml) were obtained from the Boston Children's Hospital viral vector core. The SweetieTS2 sensor is a modestly improved version of a lifetime-readout glucose sensor that we reported previously; see Fig. S8.[105] Intracranial injections for juvenile mice and hippocampal slice preparation were performed as previously described. Experiments were performed at ~34°C in a recording chamber continuously supplied with oxygenated artificial cerebrospinal fluid (aCSF) [120 mM NaCl, 2.5 mM KCl, 1 mM NaH_2PO_4, 26 mM $NaHCO_3$, 2 mM $CaCl_2$, 1 mM $MgCl_2$, 10 mM glucose] at the beginning. For P_i titrations, we used aCSF modified with either 0 or 5 mM NaH_2PO_4.

For our stimulation experiments, we only used slices where we could observe a stable baseline Pi-Tq lifetime and analyzed only cells with low baseline Ca^{2+} levels when we co-monitored RCaMP1h. For stimulation with 50 mM KCl, we used a modified aCSF with 50 mM KCl and 72.5 mM NaCl (to preserve osmolarity), which we applied for 1 minute. For electrical stimulation experiments, DGCs were stimulated synaptically (60 pulses, 20 Hz, 100–500 μA) by placing the electrode in the molecular layer, as previously described.[6]

For 0-Ca^{2+} experiments, we used a calcium-free aCSF [120 mM NaCl, 2.5 mM KCl, 1 mM NaH_2PO_4, 26 mM $NaHCO_3$, 10 mM glucose, 4.1 mM $MgCl_2$, 1 mM EGTA] for baseline recordings, based on our prior work.[11] We stimulated cells with a 1 min application of 50 mM KCl in the presence or absence of external Ca^{2+}, performing only a single stimulation per slice to avoid potential confounding effects of repeated stimulations.

Brain slice experiments were performed using the customized two-photon microscope described above, as in our prior work. We used a digital zoom factor of 1.5 – 3x, the excitation wavelength was 790 nm, and images were acquired every 15–30 seconds. We imaged soma in these experiments. Data were analyzed in custom MATLAB R2014b software. We adjusted the measured green fluorescence lifetimes in experiments where RCaMP1h were co-expressed because there is a small amount of a low-lifetime RCaMP1h intermediate with green fluorescence. We did not observe differences in baseline fluorescence lifetime between cells expressing Pi-Tq alone and Pi-Tq along with RCaMP1h (Figs. 4, S4).

In vivo imaging:

In vivo imaging experiments were conducted in awake, unanesthetized mice. Mice (postnatal day ~60–80) underwent surgical procedures as described previously.[6] Cranial window surgeries were conducted over the primary somatosensory (barrel field) cortex.[106] Four intracranial injections (~150 nl per injection, ~8 min per injection) of a solution containing either a 1:1 mixture of AAV2/9.hSyn.Pi-Tq (obtained from the Janelia Viral Tools facility, 1.8E13 GC/ml) and AAV2/9.hSyn.ChrimsonR-tdTomato (Addgene #59171, 2.2E13 GC/ml) or AAV2/9.hSyn.Pi-Tq alone were made near the center of the craniotomy, ~400 μm apart, at a depth of ~450–500 μm below the dural surface. The surface of the exposed tissue was then covered with a 4 mm diameter coverslip glued to a 5 mm diameter coverslip and cemented to the skull. Imaging experiments began approximately 20 days post-surgery to allow for proper recovery, habituation, and steady-state expression of sensors. Mice whose windows showed significant regrowth were excluded. Imaging sessions lasted 1–2 hours. The viral expression strategy permitted recording of different FOVs in the same mice over different days (at least 2 days apart).

Optogenetic activation in the cortex was conducted using full-field red light delivered through the objective at 10 ms pulse duration and 20 Hz for 30 s at a power of ~8–11 mW at the objective; stimulation was repeated over 4 to 8 trials, triggered using custom Arduino scripts. Lifetime imaging data were acquired with a modified Thorlabs Bergamo II microscope equipped with hybrid photodetectors. The two-photon excitation light source was a tunable SpectraPhysics MaiTai DeepSee mode-locked at 80 MHz. The objective lens used for in vivo imaging was a Nikon 16x LWD 0.8 NA objective. An excitation wavelength of 800 nm was used for imaging Pi-Tq. Emission light was split with an FF562-Di03 dichroic mirror and bandpass filtered for Pi-Tq (FF01–475/35) and tdTomato (FF01–641/75) channels. Fluorescence lifetimes were determined from time-correlated single photon counting data as previously described. ChrimsonR-tdTomato expression lowered the apparent Pi-Tq lifetime, likely because of immature red fluorescent protein that produces green fluorescence.[107] We therefore reported changes in Pi-Tq lifetime relative to baseline, rather than absolute lifetime, for our optogenetic stimulation experiments. For our *in vivo* experiments, we did not extrapolate the measured lifetime to P_i concentration because we did not rigorously co-monitor temperature.

Enzymatic assays:

Recombinant human PFKP (kind gift of B. Webb, WVU) was used for enzyme assays. Coupled enzymatic reactions were performed at ~25°C and at pH 7.4. For Fig. 6B, the reactions contained 3.5 mM ATP, 0.1 mM fructose 6-phosphate, 0.5–10 mM sodium phosphate, 0.15 mM NADH, 1 mM DTT, 5 mM $MgCl_2$, and 0.24 mM sodium citrate (giving free [Mg^{2+}] of ~0.6 mM and free [citrate] of ~0.1 mM). For Fig. 6C, we lowered free citrate to ~35 μM. In all cases, we used a coupled enzyme assay with 0.675 U/mL aldolase from rabbit muscle, 5 U/mL triose phosphate isomerase from rabbit muscle, and 2 U/mL glycerol phosphate dehydrogenase from rabbit muscle; auxiliary enzymes were desalted before use, as described.[63,69] Reactions were initiated with the addition of PFKP, and then absorbance at 340 nm was monitored for 15–20 minutes using a BioTek Synergy H1 plate reader. Initial velocities were measured, and kinetic parameters were determined by nonlinear regression in GraphPad Prism 10 using a Hill equation with variable slope.

Supplementary Material

Refer to Web version on PubMed Central for supplementary material.

ACKNOWLEDGMENTS:

We thank J. Davis for letting us use his fluorometer; B. Webb for providing purified PFK protein; T. Clark, M. Karkoski, and L. Silva for assistance with injections. CG is an investigator of the Howard Hughes Medical Institute. Funding was provided by fellowships to PR (Stuart H. Q. and Victoria Quan Fellowship in Neurobiology, NIH F31 CA254162) and SS (HHMI Fellowship from the Jane Coffin Childs Fund, Brain & Behavior Research Foundation Young Investigator Grant, Edward R. and Anne G. Lefler Center Postdoctoral Fellowship, Alice and Joseph Brooks Fund Postdoctoral Fellowship), and NIH grants (R01 GM124038, R37 NS102586) to GY.

REFERENCES:

1. Yellen G Fueling thought: Management of glycolysis and oxidative phosphorylation in neuronal metabolism. J Cell Bio 217:2235–2246 (2018). [PubMed: 29752396]
2. Harris JJ, Jolivet R, Attwell D. Synaptic Energy Use and Supply. Neuron 75:762–777 (2012). [PubMed: 22958818]
3. Howarth C, Gleeson P, Attwell D. Updated Energy Budgets for Neural Computation in the Neocortex and Cerebellum. J Cereb Blood Flow Metab 32:1222–1232 (2012). [PubMed: 22434069]
4. Yu Y, Herman P, Rothman DL, Agarwal D, Hyder F. Evaluating the gray and white matter energy budgets of human brain function. J Cereb Blood Flow Metab 38:1339–1353 (2018). [PubMed: 28589753]
5. Dienel GA. Brain Glucose Metabolism: Integration of Energetics with Function. Physiol Rev 99:949–1045 (2019). [PubMed: 30565508]
6. Díaz-García CM, Mongeon R, Lahmann C, Koveal D, Zucker H, Yellen G. Neuronal Stimulation Triggers Neuronal Glycolysis and Not Lactate Uptake. Cell Metab 26:361–374 (2017). [PubMed: 28768175]
7. Díaz-García CM, Meyer DJ, Nathwani N, Rahman M, Martinez-Francois JR, Yellen G. The distinct roles of calcium in rapid control of neuronal glycolysis and the tricarboxylic acid cycle. eLife 10:e64821 (2021). [PubMed: 33555254]
8. Rangaraju V, Calloway N, Ryan TA. Activity-Driven Local ATP Synthesis Is Required for Synaptic Function. Cell 156:825–835 (2014). [PubMed: 24529383]
9. Li H, Cuglielmetti C, Sei YJ, Zilberter M, Le Page LM, Shields L, Yang J, Nguyen K, Tiret B, Gao X, Bennett N, Lo I, Dayton TL, Kampmann M, Huang Y, Rathmell JC, Vander Heiden M, Chaumeil

MM, Nakamura K. Neurons require glucose uptake and glycolysis *in vivo*. Cell Rep 42:112335 (2023). [PubMed: 37027294]

10. Wolfe AD, Koberstein JN, Smith CB, Stewart ML, Gonzalez IJ, Hammarlund M, Hyman AA, Stork PJS, Goodman RH, Colón-Ramos DA. Local and dynamic regulation of neuronal glycolysis in vivo. Proc Natl Acad Sci 121:e2314699121 (2024). [PubMed: 38198527]
11. Meyer DJ, Díaz-García CM, Nathwani N, Rahman M, Yellen G. The Na^+/K^+ pump dominates control of glycolysis in hippocampal dentate granule cells. eLife 11:e81645 (2022). [PubMed: 36222651]
12. Dhar-Chowdhury P, Malester B, Rajacic P, Coetzee WA. The regulation of ion channels and transporters by glycolytically derived ATP. Cell Mol Life Sci 64:3069–3083 (2007). [PubMed: 17882378]
13. Berg JM, Tymoczko JT, Stryer L. Biochemistry, 7th ed. (2011).
14. Connett RJ, Sahlin K. Control of glycolysis and glycogen metabolism. In: Rowell Lb, Shepherd Jt., eds. Exercise: Regulation and Integration of Multiple Systems. New York: Oxford Univ. Press (1996).
15. Wegener G, Krause U. Different modes of activating phosphofructokinase, a key regulatory enzyme of glycolysis, in working vertebrate muscle. Biochem Soc Trans 30:264–270 (2002). [PubMed: 12023862]
16. Rosen PC, Fu P, Ferrán B, Kim E, Brooks DJ, Lim DC, Díaz-García CM, Yellen G. Activity-dependent citrate dynamics in neurons. Proc Natl Acad Sci 122:e2519902122 (2025). [PubMed: 41071660]
17. Reinhardt GD, Lardy HA. Rat Liver Phosphofructokinase: Kinetic Activity under Near-Physiological Conditions. Biochemistry 19:1477–1484 (1980). [PubMed: 6446316]
18. Bañuelos M, Gancedo G, Gancedo JM. Activation by Phosphate of Yeast Phosphofructokinase. J Biol Chem 252:6394–6398 (1977). [PubMed: 19473]
19. Lagunas R, Gancedo C. Role of phosphate in the regulation of the Pasteur effect in *Saccharomyces cerevisiae*. Eur J Biochem 137:479–483 (1983). [PubMed: 6229402]
20. Tsai MY, Kemp RG. Rabbit brain phosphofructokinase. J Biol Chem 249:6590–6596 (1974). [PubMed: 4371165]
21. Passonneau JV, Lowry OH. Phosphofructokinase and the Pasteur effect. Biochem Biophys Res Commun 7:10–15 (1962). [PubMed: 14484231]
22. Lowry OH, Passonneau JV. Kinetic Evidence for Multiple Binding Sites on Phosphofructokinase. J Biol Chem 241:2268–2279 (1966). [PubMed: 4223639]
23. Kushmerick MJ, Moreland TS, Wiseman RW. Mammalian skeletal muscle fibers distinguished by contents of phosphocreatine, ATP, and P_i. Proc Natl Acad Sci 89:7521–7525 (1992). [PubMed: 1502163]
24. Chance B, Leigh JS Jr, Kent J, McCully K, Nioka S, Clark BJ, Maris JM, Graham T. Multiple controls of oxidative metabolism in living tissues as studied by phosphorus magnetic resonance. Proc Natl Acad Sci 83:9458–9462 (1986). [PubMed: 3467315]
25. Roberts JKM, Wade-Jardetzky N, and Jardetzky O. Intracellular pH measurements by ^{31}P nuclear magnetic resonance. Influence of factors other than pH on ^{31}P chemical shifts. Biochemistry 20:5389–5394 (1981). [PubMed: 7295683]
26. Gest AMM, Sahan AZ, Zhong Y, Lin W, Mehta S, Zhang J. Molecular Spies in Action: Genetically Encoded Fluorescent Biosensors Light up Cellular Signals. Chem Rev 124:12573–12660 (2024). [PubMed: 39535501]
27. Mongeon R, Yellen G. Quantitative two-photon imaging of fluorescent biosensors. Curr Opin Chem Biol 27:24–30 (2015). [PubMed: 26079046]
28. Koveal DM, Díaz-García CM, Yellen G. Fluorescent biosensors for neuronal metabolism and the challenges of quantitation. Curr Opin Neurobiol 63:111–121 (2020). [PubMed: 32559637]
29. Mukherjee P, Banerjee S, Wheeler A, Ratliff LA, Irigoyen S, Garcia LR, Lockless SW, Versaw WK. Live Imaging of Inorganic Phosphate in Plants with Cellular and Subcellular Resolution. Plant Physiol 167:628–638 (2015). [PubMed: 25624397]

30. Gu H, Lalonde S, Okumoto S, Looger LL, Scharff-Poulsen AM, Grossman AR, Kossmann J, Jakobsen I, Frommer WB. A novel analytical method for in vivo phosphate tracking. FEBS Lett 580:5885–5893 (2006). [PubMed: 17034793]
31. Hrvatin S, Hochbaum DR, Nagy MA, Cicconet M, Robertson K, Cheadle L, Zilionis R, Ratner A, Borges-Monroy R, Klein AM, Sabatini BL, Greenberg ME. Single-cell analysis of experience-dependent transcriptomic states in the mouse visual cortex. Nat Neuro 21:120–129 (2018).
32. Zeisel A, Hochgerner H, Lönnerberg P, Johnsson A, Memic F, van der Zwan J, Häring M, Braun E, Borm LE, La Manno G, Codeluppi S, Furlan A, Lee K, Skene N, Harris KD, Hjerling-Leffler J, Arenas E, Ernfors P, Marklund U, Linnarsson S. Molecular Architecture of the Mouse Nervous System. Cell 174:999–1014 (2018). [PubMed: 30096314]
33. Yao Z, van Velthoven CTJ, Nguyen TN, Goldy J, Sedeno-Cortes AE, Baftizadeh F, Bertagnolli D, Casper T, Chiang M, Crichton K, Ding S, Fong O, Garren E, Glandon A, Gouwens NW, Gray J, Graybuck LT, Hawrylycz MJ, Hirschstein D, Kroll M, Lathia K, Lee C, Levi B, McMillen D, Mok S, Pham T, Ren Q, Rimorin C, Shapovalova N, Sulc J, Sunkin SM, Tieu M, Torkelson A, Tung H, Ward K, Dee N, Smith KA, Tasic B, Zeng H. A taxonomy of transcriptomic cell types across the isocortex and hippocampal formation. Cell 184:3222–3241 (2021). [PubMed: 34004146]
34. Dzeja PP, Terzic A. Phosphotransfer networks and cellular energetics. J Exp Biol 206:2039–2047 (2003). [PubMed: 12756286]
35. Erecińska M, Silver IA. ATP and Brain Function. J Cereb Blood Flow Metab 9:2–19 (1989). [PubMed: 2642915]
36. Connett RJ. Analysis of metabolic control: new insights using scaled creatine kinase model. Am J Physiol 254:R949–R959 (1988). [PubMed: 2837918]
37. Salford LG, Siesjö BK. The Influence of Arterial Hypoxia and Unilateral Carotid Artery Occlusion upon Regional Blood Flow and Metabolism in the Rat Brain. Acta Phys 92:130–141 (1974).
38. Hope PL, Cady EB, Chu A, Delpy DT, Gardiner RM, Reynolds EO. Brain Metabolism and Intracellular pH During Ischaemia and Hypoxia: An *In Vivo* ^{31}P and ^{1}H Nuclear Magnetic Resonance Study in the Lamb. J Neurochem 49:75–82 (1987). [PubMed: 3585343]
39. Rango M, Castelli A, Scarlato G. Energetics of 3.5 s Neural Activation in Humans: a ^{31}P MR Spectroscopy Study. Magn Res Med 38:878–883 (1997).
40. Sappy-Marinier D, Calabrese G, Fein G, Hugg JW, Biggins C, Weiner MW. Effect of Photic Stimulation on Human Visual Cortex Lactate and Phosphates Using ^{1}H and ^{31}P Magnetic Resonance Spectroscopy. J Cereb Blood Flow Metab 12:584–592 (1992). [PubMed: 1618937]
41. Sahlin K, Söderlund K, Tonkonogi M, Hirakoba K. Phosphocreatine content in single fibers of human muscle after sustained submaximal exercise. Am J Physiol Cell Physiol 273:C172–C178 (1997).
42. Mörikofer-Zwez S, Walter P. Binding of ADP to rat liver cytosolic proteins and its influence on the ratio of free ATP/free ADP. Biochem J 269:117–124 (1989).
43. Goedhart J, von Stetten D, Noirclerc-Savoye M, Lelimousin M, Joosen L, Hink MA, van Weeren L, Gadella TWJ Jr., Royant A Structure-guided evolution of cyan fluorescent proteins towards a quantum yield of 93%. Nat Commun 3:571 (2012).
44. van der Linden FH, Mahlandt EK, Arts JJG, Beumer J, Puschhof J, de Man SMA, Chertkova AO, Ponsioen B, Clevers H, van Buul JD, Postma M, Gadella TWJ Jr, Goedhart J. A turquoise fluorescence lifetime-based biosensor for quantitative imaging of intracellular calcium. Nat Commun 12:7159 (2022).
45. Zhong C, Arai S, Okada Y. Development of fluorescence lifetime biosensors for ATP, cAMP, citrate, and glucose using the mTurquoise2-based platform. Cell Rep Methods 4:100902 (2024). [PubMed: 39561716]
46. Jennings ML. Role of transporters in regulating mammalian intracellular inorganic phosphate. Front Pharmacol 14:1163442 (2023). [PubMed: 37063296]
47. Hawkins RA, Nielsen RC, Veech RL. The measurement of the inorganic phosphate content of brain in the presence of bone fragments. J Neurochem 20:35–38 (1973). [PubMed: 4347047]
48. Veech RL, Lawson JW, Cornell NW, Krebs HA. Cytosolic phosphorylation potential. J Biol Chem 254:6538–6547 (1979). [PubMed: 36399]

49. Tantama M, Martínez-François JR, Mongeon R, Yellen G. Imaging energy status in live cells with a fluorescent biosensor of the intracellular ATP-to-ADP ratio. Nat Commun 4:2550 (2013). [PubMed: 24096541]
50. Imamura H, Huynh Nhat KP, Togawa H, Saito K, Iino R, Kato-Yamada Y, Nagai T, Noji H. Visualization of ATP levels inside single living cells with fluorescence resonance energy transfer-based genetically encoded indicators. Proc Natl Acad Sci 106:15651–15656 (2009). [PubMed: 19720993]
51. Marvin JS, Kokotos AC, Kumar M, Pulido C, Tkachuk AN, Yao JS, Brown TA, Ryan TA. iATPSnFR2: A high-dynamic-range fluorescent sensor for monitoring intracellular ATP. Proc Natl Acad Sci 121:e2314604121 (2024). [PubMed: 38748581]
52. Lerchundi R, Huang N, Rose CR. Quantitative Imaging of Changes in Astrocytic and Neuronal Adenosine Triphosphate Using Two Different Variants of ATeam. Front Cell Neuro 14:80 (2020).
53. Straub I, Kunstmann L, Baeza-Lehnert F, Chowdhry S, Renden RB, Gonzalez-Aragón G, Groschup B, Hofmann T, Jovanović S, Sonntag M, Gitler D, Schaefer M, Eilers J, Barros LF, Hirrlinger J, Hallermann S. Presynaptic ATP Decreases During Physiological-Like Activity in Neurons Tuned for High-Frequency Transmission. J Neurochem 169:e70212 (2025). [PubMed: 40916622]
54. Zampese E, Wokosin DL, Gonzalez-Rodriguez P, Guzman JN, Tkatch T, Kondapalli J, Surmeier WC, D'Alessandro KB, De Stefani D, Rizzuto R, Iino M, Molkentin JD, Chandel NS, Schumacker PT, Surmeier DJ. Ca2+ channels couple spiking to mitochondrial metabolism in substantia nigra dopaminergic neurons. Sci Adv 8:eabp8701 (2022). [PubMed: 36179023]
55. Okawa H, Sampath AP, Laughlin SB, Fain GL. ATP Consumption by Mammalian Rod Photoreceptors in Darkness and in Light. Curr Biol 18:1917–1921 (2008). [PubMed: 19084410]
56. Gerkau NJ, Lerchundi R, Nelson JSE, Lantermann M, Meyer J, Hirrlinger J, Rose CR. Relation between activity-induced intracellular sodium transients and ATP dynamics in mouse hippocampal neurons. J Physiol 597:5687–5705 (2019). [PubMed: 31549401]
57. Baeza-Lehnert F, Saab AS, Gutiérrez R, Larenas V, Díaz E, Horn M, Vargas M, Hösli L, Stobart J, Hirrlinger J, Weber B, Barros LF. Non-Canonical Control of Neuronal Energy Status by the Na^+ Pump. Cell Metab 29:668–680 (2019). [PubMed: 30527744]
58. Akerboom J, Carreras Calderón N, Tian L, Wabnig S, Prigge M, Tolö J, Gordus A, Orger MB, Severi KE, Macklin JJ, Patel R, Pulver SR, Wardill TJ, Fischer E, Schüler C, Chen TW, Sarkisyan KS, Marvin JS, Bargmann CI, Kim DS, Kügler S, Lagnado L, Hegemann P, Gottschalk A, Schreiter ER, Looger LL. Genetically encoded calcium indicators for multi-color neural activity imaging and combination with optogenetics. Front. Mol. Neuro 6:2 (2013).
59. Klapoetke NC, Murata Y, Kim SS, Pulver SR, Birdsey-Benson A, Cho YK, Morimoto TK, Chuong AS, Carpenter EJ, Tian Z, Wang J, Xie Y, Yan Z, Zhang Y, Chow BY, Surek B, Melkonian M, Jayaraman V, Constantine-Paton M, Wong GK, Boyden ES. Independent optical excitation of distinct neural populations. Nat Methods 11:338–346 (2014). [PubMed: 24509633]
60. Bottomley PA, Charles HC, Roemer PB, Flamig S, Engeseth H, Edelstein WA, Mueller OM. Human in vivo phosphate metabolite imaging with 31P NMR. Magn Res Med 7:319–336 (1988).
61. Choe M, Einav T, Phillips R, Titov DV. Glycolysis model shows that allostery maintains high ATP and limits accumulation of intermediates. Biophys J 124:1562–1586 (2025). [PubMed: 40186355]
62. Herrero-Mendez A, Almeida A, Fernández E, Maestre C, Moncada S, Bolaños JP. The bioenergetic and antioxidant status of neurons is controlled by continuous degradation of a key glycolytic enzyme by APC/C–Cdh1. Nat Cell Bio 11:747–752 (2009). [PubMed: 19448625]
63. Voronkova MA, Hansen HL, Cooper MP, Miller J, Sukumar N, Geldenhuys WJ, Robart AR, Webb BA. Cancer-associated somatic mutations in human phosphofructokinase-1 reveal a critical electrostatic interaction for allosteric regulation of enzyme activity. Biochem J 480:1411–1427 (2023). [PubMed: 37622331]
64. Foe LG, Kemp RG. Isolation and Characterization of Phosphofructokinase C from Rabbit Brain. J Biol Chem 260:726–730 (1985). [PubMed: 3155729]
65. DeVivo DC, Leckie MP, Ferrendelli JS, McDougal DB. Chronic Ketosis and Cerebral Metabolism. Ann Neurol 3:331–337 (1978). [PubMed: 666275]

66. Lowry OH, Passonneau JV. The Relationships between Substrates and Enzymes of Glycolysis in Brain. J Biol Chem 239:31–42 (1964). [PubMed: 14114860]

67. Wu TL, Davis EJ. Regulation of glycolytic flux in an energetically controlled cell-free system: The effects of adenine nucleotide ratios, inorganic phosphate, pH, and citrate. Arch Biochem Biophys 209:85–99 (1981). [PubMed: 6456696]

68. Li Y, Rivera D, Ru W, Gunasakera D, Kemp RG. Identification of Allosteric Sites in Rabbit Phosphofructo-1-kinase. Biochemistry 38:16407–16412 (1999). [PubMed: 10587466]

69. Webb BA, Forouhar F, Szu F, Seetharaman J, Tong L, Barber DL. Structures of human phosphofructokinase-1 and atomic basis of cancer-associated mutations. Nature 523:111–114 (2015). [PubMed: 25985179]

70. Lynch EM, Hansen H, Salay L, Cooper M, Timr S, Kollman JM, Webb BA. Structural basis for allosteric regulation of human phosphofructokinase-1. Nat Commun 15:7323 (2024). [PubMed: 39183237]

71. Michigami T, Kawai M, Yamazaki M, Ozono K. Phosphate as a Signaling Molecule and Its Sensing Mechanism. Physiol Rev 98:2317–2348 (2018). [PubMed: 30109818]

72. Santos-Beneit F The Pho regulon: a huge regulatory network in bacteria. Front Microbiol 6:402 (2015). [PubMed: 25983732]

73. Ljungdahl PO, Daignan-Fornier B. Regulation of Amino Acid, Nucleotide, and Phosphate Metabolism in Saccharomyces cerevisiae. Genetics 190:885–929 (2012). [PubMed: 22419079]

74. Xu C, Xu J, Tang H, Ericsson M, Weng J, DiRusso J, Hu Y, Ma W, Asara JM, Perrimon N. A phosphate-sensing organelle regulates phosphate and tissue homeostasis. Nature 617:798–806 (2023). [PubMed: 37138087]

75. Bru S, Mayer LM, Kim G, Qiu D, Jessen HJ, Mayer A. Acidocalcisome-like vacuoles constitute a feedback-controlled phosphate buffering system for the cytosol. eLife 14: RP108181 (2025). [PubMed: 41324358]

76. Yan R, Chen H, Liu C, Zhao J, Wu D, Jiang J, Gong J, Jiang D. Human XPR1 structures reveal phosphate export mechanism. Nature 633:960–967 (2024). [PubMed: 39169184]

77. Lu Y, Yue C, Zhang L, Yao D, Xia Y, Zhang Q, Zhang X, Li S, Shen Y, Cao M, Guo C, Qin A, Zhao J, Zhou L, Yu Y, Cao Y. Structural basis for inositol pyrophosphate gating of the phosphate channel XPR1. Science 386:eadp3252 (2024). [PubMed: 39325866]

78. Cheng X, Zhao M, Chen L, Huang C, Xu Q, Shao J, Wang H, Zhang Y, Li X, Xu X, Yao X, Lin K, Xue H, Wang H, Chen Q, Zhu Y, Zhou J, Ge W, Zhu S, Liu J, Chen W, Xiong Z. Astrocytes modulate brain phosphate homeostasis via polarized distribution of phosphate uptake transporter PiT2 and exporter XPR1. Neuron 112:3126–3142 (2024). [PubMed: 39019040]

79. Ouyang Y, Jeong M, Cunningham CN, Berg JA, Toshniwal AG, Hughes CE, Seiler K, Van Vranken JG, Cluntun AA, Lam G, Winter JM, Akdogan E, Dove KK, Nowinski SM, West M, Odorizzi G, Gygi SP, Dunn CD, Winge DR, Rutter J. Phosphate starvation signaling increases mitochondrial membrane potential through respiration-independent mechanisms. eLife 13:e84282 (2024). [PubMed: 38251707]

80. Wolf SG, Mutsafi Y, Dadosh T, Ilani T, Lansky Z, Horowitz B, Rubin S, Elbaum M, Fass D. 3D visualization of mitochondrial solid-phase calcium stores in whole cells. eLife (2017).

81. Lehninger AL. Role of Phosphate and Other Proton-Donating Anions in Respiration-Coupled Transport of Ca^{2+} by Mitochondria. Proc Natl Acad Sci 71:1520–1524 (1974). [PubMed: 4364542]

82. Rae CD, Bröer S. Creatine as a booster for human brain function. How might it work? Neurochem Int 89:249–259 (2015). [PubMed: 26297632]

83. Ho T, Potapenko E, Davis DB, Merrins MJ. A plasma membrane-associated glycolytic metabolon is functionally coupled to K_{ATP} channels in pancreatic α and β cells from humans and mice. Cell Rep 42:112394 (2023). [PubMed: 37058408]

84. Jang S, Nelson JC, Bend EG, Ródriguez-Laureano L, Tueros FG, Cartagenova L, Underwood K, Jorgensen EM, Colón-Ramos DA. Glycolytic Enzymes Localize to Synapses under Energy Stress to Support Synaptic Function. Science 90:278–291 (2016).

85. Fell DA. Metabolic Control Analysis: a survey of its theoretical and experimental development. Biochem J 286:313–330 (1992). [PubMed: 1530563]

86. Kokotos AC, Antoniazzi AM, Unda SR, Ko MS, Park S, Eliezer D, Kaplitt MG, De Camilli P, Ryan TA. Phosphoglycerate kinase is a central leverage point in Parkinson's disease–driven neuronal metabolic deficits. Sci Adv 10:eadn6016 (2024). [PubMed: 39167658]

87. Shestov AA, Liu X, Ser A, Cluntun AA, Hung YP, Huang L, Kim D, Le A, Yellen G, Albeck JG, Locasale JW. Quantitative determinants of aerobic glycolysis identify flux through the enzyme GAPDH as a limiting step. eLife 3:e03342 (2014). [PubMed: 25009227]

88. Park JO, Tanner LB, Wei MH, Khana DB, Jacobson TB, Zhang Z, Rubin SA, Li SH, Higgins MB, Stevenson DM, Amador-Noguez D, Rabinowitz JD. Near-equilibrium glycolysis supports metabolic homeostasis and energy yield. Nat Chem Biol 15:1001–1008 (2019). [PubMed: 31548693]

89. Singh M, Wolfe AD, Vishwanath AA, Tsives A, Gonzalez IJ, Emerson SE, Goodman R, Colón-Ramos D. Glycogen supports glycolytic plasticity in neurons. Proc Natl Acad Sci 122:e2509003122 (2025). [PubMed: 40638090]

90. Saez I, Duran J, Sinadinos C, Beltran A, Yanes O, Tevy MF, Martínez-Pons C, Milán M, Guinovart JJ. Neurons have an active glycogen metabolism that contributes to tolerance to hypoxia. J Cereb Blood Flow Metab 34:945–55 (2014). [PubMed: 24569689]

91. Duran J, Gruart A, Varea O, López-Soldado I, Delgado-García JM, Guinovart JJ. Lack of neuronal glycogen impairs memory formation and learning-dependent synaptic plasticity in mice. Front Cell Neurosci 13:374 (2019). [PubMed: 31456667]

92. Lowry OH, Schulz DW, Passonneau JV. The Kinetics of Glycogen Phosphorylases from Brain and Muscle. J Biol Chem 242:271–280 (1967). [PubMed: 6016612]

93. Newgard CB, Hwang PK, Fletterick RJ. The Family of Glycogen Phosphorylases: Structure and Function. Crit Rev Biochem Mol Bio 24:69–99 (1989). [PubMed: 2667896]

94. Cohen P Protein phosphorylation and the control of glycogen metabolism in skeletal muscle. Philos Trans R Soc Lond B Biol Sci 302:13–25 (1983). [PubMed: 6137000]

95. Newholme EA, Rolleston FS, Taylor K. Factors affecting the Glucose 6-Phosphate Inhibition of Hexokinase from Cerebral Cortex Tissue of the Guinea Pig. Biochem J 106:193–201(1968). [PubMed: 5721456]

96. Ellison WR, Lueck JD, Fromm HJ. Studies on the mechanism of orthophosphate regulation of bovine brain hexokinase. J Biol Chem 250:1864–1871 (1975). [PubMed: 1112835]

97. Aleshin AE, Zeng C, Bartunik HD, Fromm HJ, Honzatko RB. Regulation of hexokinase I: crystal structure of recombinant human brain hexokinase complexed with glucose and phosphate. J Mol Bio 282:345–357 (1998). [PubMed: 9735292]

98. Kvamme E, Roberg B, Torgner IA. Phosphate-Activated Glutaminase and Mitochondrial Glutamine Transport in the Brain. Neurochem Res 25:1407–1419 (2000). [PubMed: 11059811]

99. Mootha VK, Arai AE, Balaban RS. Maximum oxidative phosphorylation capacity of the mammalian heart. Am J Physiol 272:H769–775 (1997). [PubMed: 9124437]

100. Hyder F, Rothman DL. Advances in imaging brain metabolism. Ann Rev Biomed Eng 19:485–515 (2017). [PubMed: 28633562]

101. Miller A, York EM, Stopka SA, Martínez-François JR, Hossain MA, Baquer G, Regan MS, Agar NYR, Yellen G. Spatially resolved metabolomics and isotope tracing reveal dynamic metabolic responses of dentate granule neurons with acute stimulation. Nat Metab 5:1820–1835 (2023). [PubMed: 37798473]

102. Yang X, Heinemann M, Howard J, Huber G, Iyer-Biswas S, Le Treut G, Lynch M, Montooth KL, Needleman DJ, Pigolotti S, Rodenfels J, Ronceray P, Shankar S, Tavassoly I, Thutupalli S, Titov DV, Wang J, Foster PJ. Physical bioenergetics: Energy fluxes, budgets, and constraints in cells. Proc Natl Acad Sci 118:e2026786118 (2021). [PubMed: 34140336]

103. Hoops S, Sahle S, Gauges R, Lee C, Pahle J, Simus N, Singhal M, Xu L, Mendes P, Kummer U. COPASI—a COmplex PAthway Simulator. Bioinformatics 22:3067–3074 (2006). [PubMed: 17032683]

104. Abramson J, Adler J, Dunger J, Evans R, Green T, Pritzel A, Ronneberger O, Willmore L, Ballard AJ, Bambrick J, Bodenstein SW, Evans DA, Hung C-C, O'Neill M, Reiman D, Tunyasuvunakool K, Wu A, Žemgulytė A, Arvaniti E, Beattie C, Bertolli O, Bridgland A, Cherepanov A, Congreve M, Cowen-Rivers AI, Cowie A, Figurnov M, Fuchs FB, Gladman H, Jain R, Khan YA, Low

CMR, Perlin K, Potapenko A, Savy P, Singh S, Stecula A, Thillaisundaram A, Tong C, Yakneen S, Zhong ED, Zielinski M, Žídek A, Bapst V, Kohli P, Jaderberg M, Hassabis D, Jumper JM. Accurate structure prediction of biomolecular interactions with AlphaFold 3. Nature 630:493–500 (2024). [PubMed: 38718835]

105. Díaz-García CM, Lahmann C, Martínez-François JR, Li B, Koveal D, Nathwani N, Rahman M, Keller JP, Marvin JS, Looger LL, Yellen G. Quantitative in vivo imaging of neuronal glucose concentrations with a genetically encoded fluorescence lifetime sensor. J Neurosci Res 97:946–960 (2019). [PubMed: 31106909]
106. Krolak T, Kaplan L, Navas K, Chen L, Birmingham A, Ryvkin D, Izsa V, Powell M, Wu Z, Deverman BE, Gu C. Brain endothelial gap junction coupling enables rapid vasodilation propagation during neurovascular coupling. Cell 188:5003–5019 (2025). [PubMed: 40675149]
107. Verukhusha VV, Chudakov DM, Gurskaya NG, Lukyanov S, Lukyanov KA. Common Pathway for the Red Chromophore Formation in Fluorescent Proteins and Chromoproteins. Chem Biol 11:845–854 (2004). [PubMed: 15217617]

SIGNIFICANCE STATEMENT

Neurons rapidly change their metabolism to meet the energy demands caused by depolarization. Understanding the mechanism of this fast response has been challenging due in part to the difficulty in measuring the small-molecule regulators of metabolism dynamically in living cells. We engineered a quantitative fluorescent biosensor to measure P_i, a sensitive indicator of energy demand that can activate glycolysis. Within seconds of stimulating neurons, there are millimolar increases in cytosolic P_i, consistent with the P_i concentrations required to strongly activate glycolysis enzymes in vitro. P_i is thus an attractive candidate for quickly linking energy consumption with energy resupply in neurons.

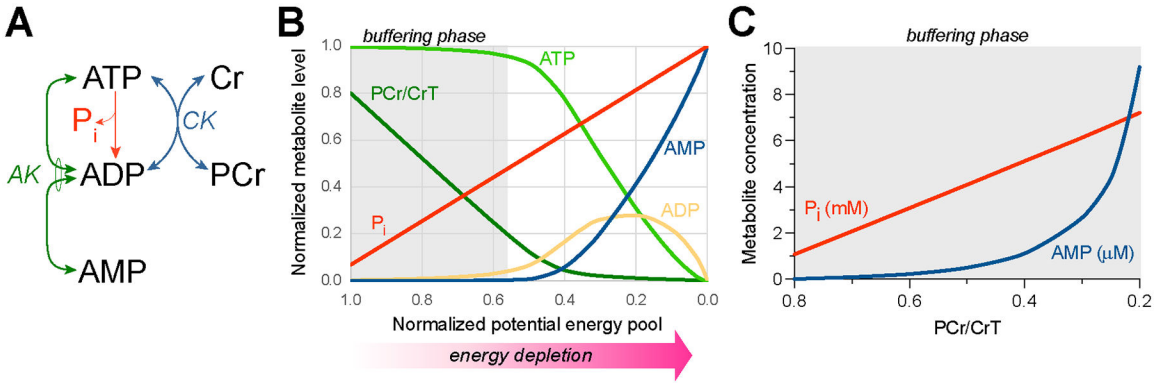

Figure 1: Inorganic phosphate is a sensitive indicator of energy demand

A) The coupled equilibrium between adenylate kinase (AK) and creatine kinase (CK), which responds to energy demand in excitable cells. **B,C)** Inorganic phosphate is a sensitive indicator of energy demand. Considering only the AK/CK equilibrium, inorganic phosphate (abbreviated as P_i, red line) increases linearly with energy demand, while ATP (light green line) is only depleted after phosphocreatine (abbreviated as PCr, dark green line) is. The buffering phase, corresponding to ΔG(ATP) values that will sustain the function of the Na^+/K^+-ATPase with nominal ion gradients (roughly −51 kJ/mol), is shown in light gray. The normalized potential energy pool reflects the fraction of available high-energy phosphate bonds. **C)** Inorganic phosphate levels are predicted to be in the low millimolar range (based on the pool sizes of phosphocreatine and ATP), while AMP levels are in the low micromolar range (based on the equilibrium constant of AK).

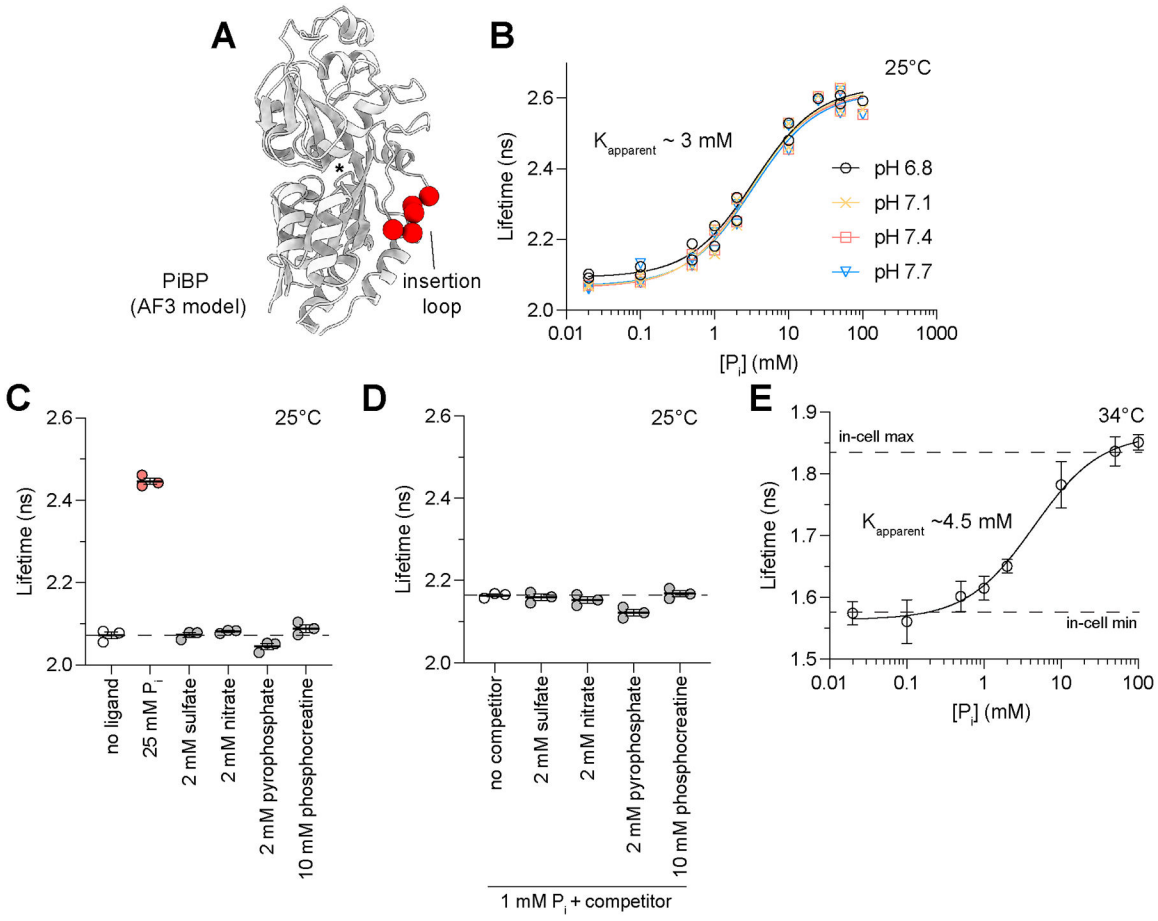

Figure 2: A robust single-color fluorescence-lifetime readout biosensor for inorganic phosphate

A) AlphaFold3-predicted model of PiBP from *Synechococcus*, with the 1.6m affinity mutations described in Ref. 29. The loop region at the back of the putative inorganic phosphate binding site (denoted with a *) that we targeted for cpTq insertion is highlighted in red spheres. **B)** Pi-Tq is pH-resistant within the physiological pH range for the cytosol (2 independent protein preparations). **C)** Inorganic phosphate, but not the related ligands sulfate, nitrate, pyrophosphate, or phosphocreatine (shown in gray), leads to an increase Pi-Tq lifetime. **D)** These ligands also do not compete with the ability of P_i to elicit a fluorescence change in Pi-Tq. The fluorescence lifetimes at 0- and 100-mM phosphate are demarcated with dotted lines. The results for **C** and **D** represent mean ± SEM for a representative protein preparation. **E)** Calibration of purified Pi-Tq protein at 34°C using two-photon excitation (mean ± SD, n=3 independent protein preparations). In permeabilized HEK293T cells transfected with pAAV-CAG-Pi-Tq, the lifetime in 0 mM extracellular P_i was 1.58 ± 0.03 ns while the lifetime in 100 mM extracellular P_i was 1.83 ± 0.03 ns (mean ± SD, n=3 independent transfections imaged on separate days), similar to the purified protein calibration. The limiting in-cell lifetimes are marked with dotted lines.

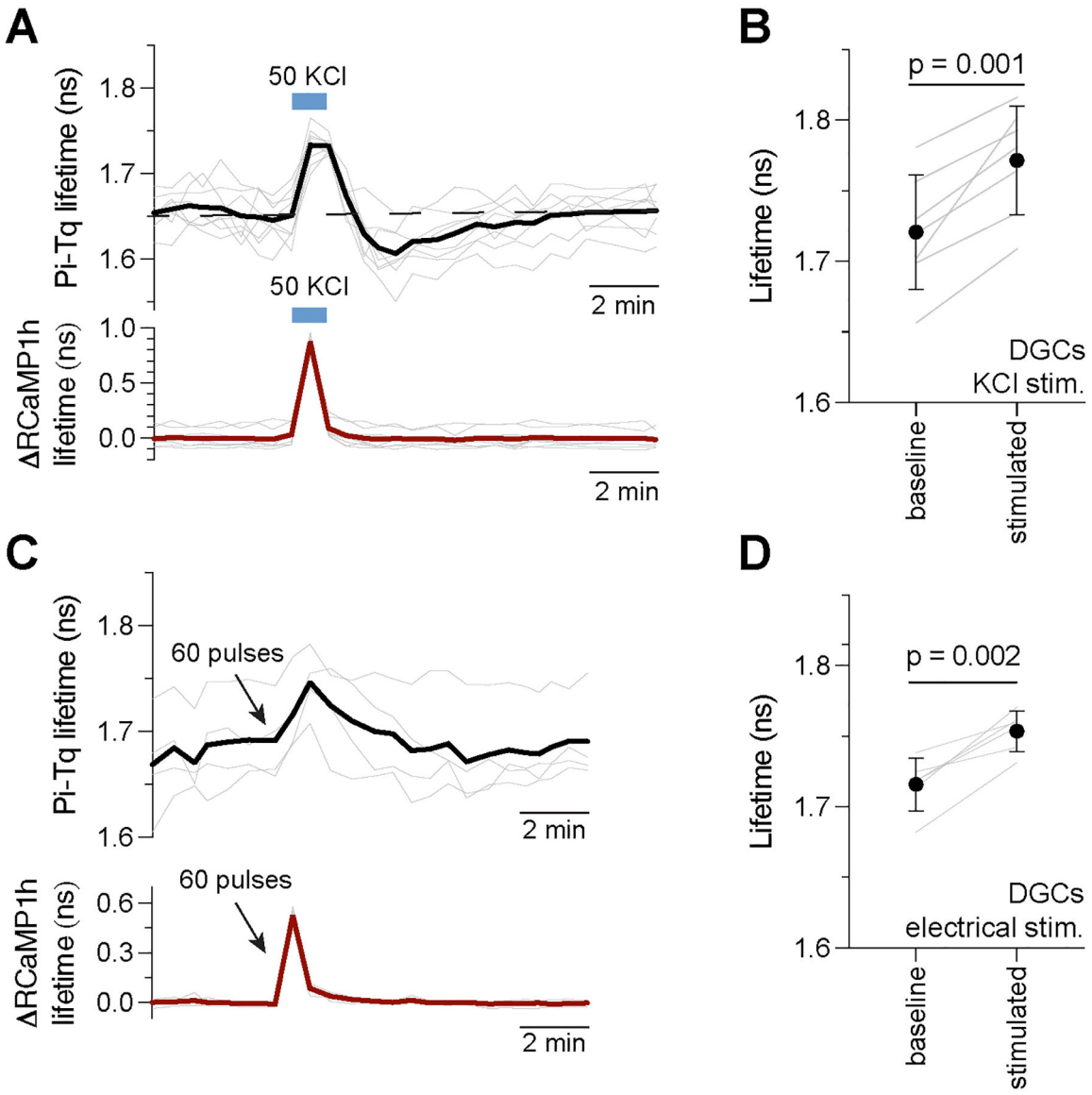

Figure 3: Activity-dependent inorganic phosphate transients in acute mouse brain slices

A,B) DGCs were depolarized with a 1-min pulse of 50 mM KCl, leading to a prompt rise in cytosolic P_i in soma that recovered back to baseline over a few minutes. A representative trace is shown in **A**; the calcium sensor RCaMP1h was co-monitored as a control for stimulation. Individual cells are shown as thin lines, and the mean for all cells in the slice is shown as a thick line. For clarity, the baseline lifetime in the Pi-Tq trace is marked with a dotted line. The undershoot in phosphate after strong stimulation is highly reproducible. Quantitation is shown in **B**, with each replicate reflecting a slice (mean ± SD; $N_{mice} = 5$, $N_{slices} = 7$, $N_{cells} = 44$). **C,D)** DGCs were electrically stimulated, eliciting a small, transient increase in cytosolic P_i. A representative trace is shown in **C**, and the results are quantified in **D** (mean ± SD; $N_{mice} = 3$, $N_{slices} = 6$, $N_{cells} = 35$). P-values in **B** and **D** were calculated using paired, two-tailed Student's t-tests.

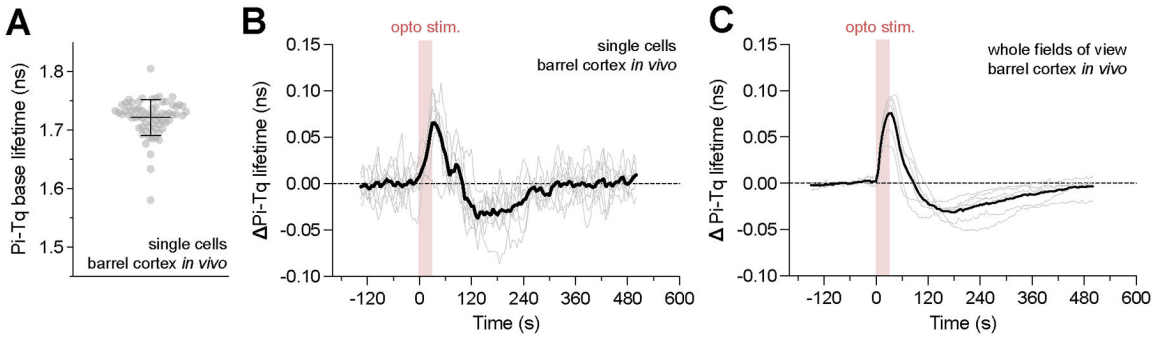

Figure 4: Inorganic phosphate transients *in vivo* with optogenetic stimulation

A) Baseline lifetime of Pi-Tq expressed in neurons in awake, head-fixed mouse barrel cortex imaged using 2pFLIM. **B,C)** Phosphate dynamics upon optogenetic stimulation. Mice were co-injected with AAVs expressing ChrimsonR-tdTomato and Pi-Tq. Neurons were optogenetically stimulated with a 30 sec pulse of red light (20Hz, 10ms pulses, pink shaded region), leading to a prompt rise in inorganic phosphate, followed by an undershoot, and then recovery back to baseline over 2–3 min. **B** shows traces from 9 individual cells (thin gray lines, with the mean shown as a thicker black line) from a representative field of view (FOV), while **C** shows a mean trace compiled from 6 mice (average trace per mouse in thin gray lines; overall mean as a thicker black line).

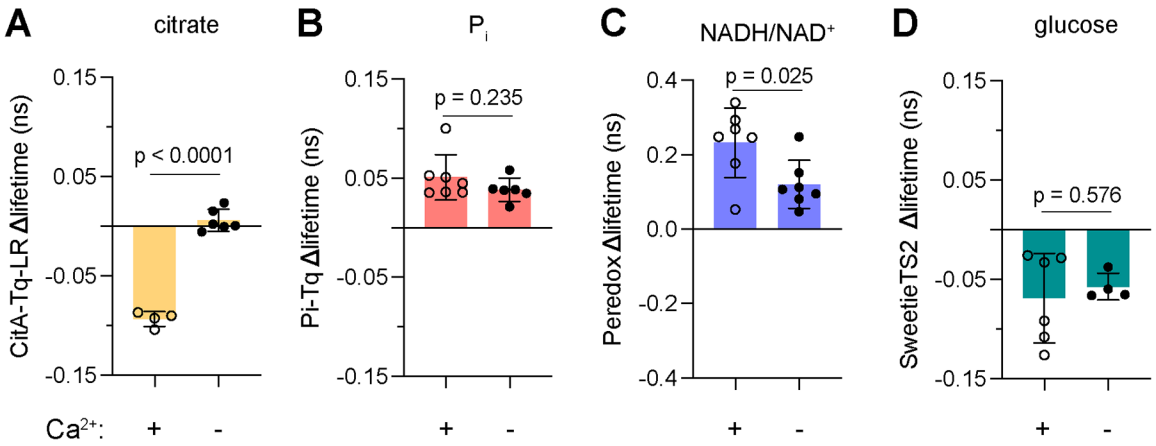

Figure 5: Signals beyond citrate regulate neuronal glycolysis

DGCs in acute mouse brain slices were depolarized with a 1-min pulse of aCSF containing 50 mM KCl in the presence (empty circles) and absence (black filled circles) of extracellular Ca^{2+}. **A)** Depolarization in the absence of Ca^{2+} eliminated the stimulation-induced dip in cytosolic citrate that we measured using CitA-Tq-LR (+ Ca^{2+}: N_{mice} = 3, N_{slices} = 4, N_{cells} = 21; - Ca^{2+}: N_{mice} = 3, N_{slices} = 6, N_{cells} = 40), **B)** but not the stimulation-induced rise in cytosolic P_i that we measured using Pi-Tq, (+ Ca^{2+}: N_{mice} =5, N_{slices} =7, N_{cells}= 44 [data from Fig. 4B]; - Ca^{2+}: N_{mice} =4, N_{slices} =7, N_{cells}= 35). **C,D)** Glycolysis is activated by depolarization in both the presence and absence of extracellular Ca^{2+}, based on measurements of **C)** the cytosolic NADH/NAD^+ ratio using Peredox (+ Ca^{2+}: N_{mice} =4, N_{slices} =7, N_{cells}= 35; - Ca^{2+}: N_{mice} =4, N_{slices} =7, N_{cells}= 35) and **D)** glucose using SweetieTS2 (N_{mice} =3, N_{slices} =6, N_{cells}= 26; - Ca^{2+}: N_{mice} =3, N_{slices} =4, N_{cells}= 16). In all cases, each replicate reflects a single slice, the mean ± SD is shown, and p-values were calculated using unpaired two-tailed Student's t-tests.

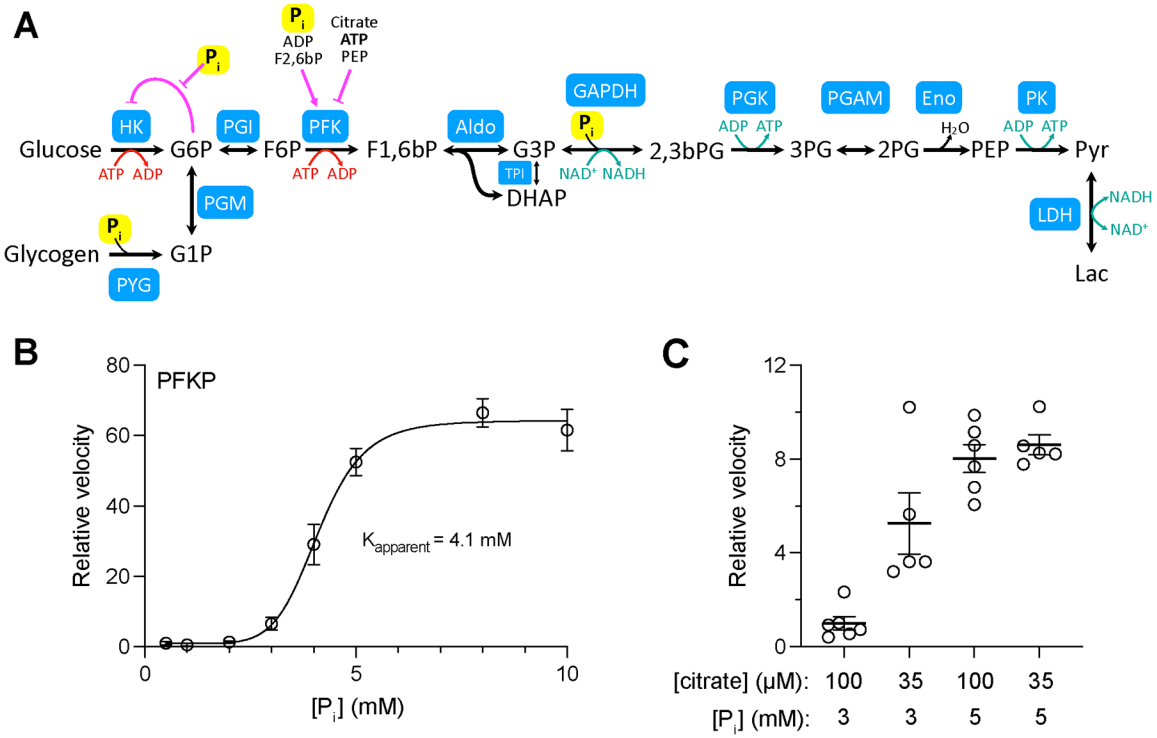

Figure 6: Inorganic phosphate activates phosphofructokinase

A) Inorganic phosphate (highlighted in yellow) activates four steps in glycolysis. As a regulator, P_i could relieve product inhibition in hexokinase or allosterically activate phosphofructokinase to increase glycolysis. As a substrate for glycogen phosphorylase (PYG) and GAPDH, P_i could also increase glycogenolysis and flux through phosphoglycerate kinase (PGK). **B)** Inorganic phosphate is a potent regulator of human PFKP under near-physiological conditions, activating it with a $K_{0.5}$ of 4.1 mM with strong cooperativity (Hill coefficient of 7.5). The results reflect mean ± SEM of 6 technical replicates. **C)** Physiological changes in citrate and P_i both activate PFK. The results reflect mean ± SEM of 5–6 technical replicates, and the points for 100 μM free citrate are the same as in **B** (normalized to the 100 μM citrate/3 mM P_i condition).